Magnon energy renormalization in yttrium iron garnet

D. S. Maior,* E. C. Souza, and S. M. Rezende
Departamento de Física, Universidade Federal de Pernambuco, 50670–901, Recife, Pernambuco, Brazil

(Received 12 April 2023; revised 29 June 2023; accepted 18 July 2023; published 7 August 2023)

Yttrium iron garnet (YIG) has been a prototype material for the study of the basic physics in magnonic and a key material for spintronics and some technological applications. For this reason, its detailed characterization is crucial for a more complete knowledge of its properties and for the understanding of phenomena in which it is involved. Here, we report a study of magnon energy renormalization on YIG utilizing Brillouin light-scattering (BLS) technique to observe the temperature dependence of the acoustic magnon mode frequency. A numerical calculation performed considering the magnon energy renormalization due to four-magnon exchange scattering shows a quite good fit to the experimental data obtained with BLS.

DOI: 10.1103/PhysRevB.108.054406

I. INTRODUCTION

The ferrimagnetic insulator yttrium iron garnet ($Y_3Fe_5O_{12}$, YIG) has played a key role in magnetism, mainly due to its very low magnetic and acoustic losses and long spin-lattice relaxation time. For several decades YIG has been the prototype material for studies of the basic physics of a variety of magnonic phenomena, such as spin-wave resonances and relaxation [1–9], propagation and processing of coherent magnon packets [6–11], microwave spin-wave instabilities [1,2,9,12], solitons [13,14], nonlinear dynamics and chaotic behavior [12,15,16], Bose-Einstein condensation of magnons [17–19], cavity magnonics [20], among others. YIG also has attracted technological attention for its possible use in many devices, such as parametric microwave amplifiers [1,21], variable delay lines [22], tunable microwave filters [23], magnetic bubble memories [24], magneto-optical devices [25], magnon transistor and logic gates [8,26], some of which led to commercial products. In the last decade YIG has gained tremendous attention as a key material in insulator-based magnon spintronics for revealing unique features of various effects, such as the spin-pumping and spin-Hall effects [27–34], spin-Seebeck, spin-Peltier, and other thermal effects [35–48], and spin-Hall magnetoresistance [49,50].

The theoretical interpretation of thermal properties and dynamic magnetic phenomena requires detailed knowledge of the magnetic excitations of the material. YIG has a complex cubic crystal structure, with 20 magnetic ferric Fe^{3+} ions occupying two inequivalent positions in the conventional body-centered cubic unit cell, with 12 pointing in one direction and 8 in the opposite one, forming a ferrimagnetic arrangement [4,51–54]. Thus, there are 20 spin-wave modes, one of them corresponding to an excitation that has all spins precessing in phase, which is called the acoustic mode, in analogy to the elastic vibration modes. The other 19 modes have higher energies and are called optical modes. The acoustic mode behaves like spin waves in a ferromagnet, and can be probed by microwave techniques and inelastic light scattering only for wave numbers $k \leqslant 5 \times 10^5$ cm^{-1}. The full dispersion relations over the whole Brillouin zone for all magnon modes can only be measured by inelastic neutron-scattering techniques. This was first done in YIG four decades ago [52,53] and comparison with the calculated dispersions [55,56] allowed determination of the exchange-interaction parameters between the spins. The initial measurements were done with limited techniques that allowed measurements of some but not all optical modes, so that only a few parameters were determined. More recently, data obtained in a modern neutron-scattering facility made possible the determination of a larger number and more precise values of the exchange parameters [54,57].

In the early calculations of the thermal magnetic properties at low temperatures, YIG was treated as a ferromagnet with a single, parabolic spin-wave dispersion [3,7]. Clearly, the correct calculation of the thermal magnetic properties at elevated temperatures has to consider that the optical magnon mode states are also populated. Such calculation has recently been done for complex ferrimagnets by computing the atomistic spin dynamics in the long (ergodic) time limit [58,59]. The calculations consider the numerically determined dispersion relations of all magnon modes and the results are in excellent agreement with experimental data. However, calculations of the thermal properties of YIG considering only the acoustic magnon mode with an improved, nonparabolic, temperature-dependent dispersion relation, give surprisingly good results even at relatively high temperatures [9,45,60]. The advantage of this approach compared to the sophisticated numerical methods is that it is accessible to a broader audience.

In this paper we present a calculation of the magnon energy renormalization based on the simple approach of Refs. [9,45] considering only the acoustic magnon mode with an improved, nonparabolic, dispersion relation. The results are used to calculate the temperature dependence of the magnetization in yttrium iron garnet and compare to the experimentally measured values. We also present the temperature dependence

*Corresponding author: daniel.soutomaior@ufpe.br

of the low wave-number magnon frequency measured with Brillouin light-scattering techniques and show that the data are well explained by calculations considering the magnon energy renormalization and the temperature dependence of the magnetization

II. THEORY FOR THE MAGNON ENERGY RENORMALIZATION

We consider the magnon system described by the Hamiltonian

$$\mathrm{H} = E_0 + \sum_k \hbar\,\omega_k c_k^\dagger c_k \;+\; \mathrm{H_{int}}, \tag{1}$$

where the first term is a ground-state energy, the second term represents a collection of independent boson excitations, in which $c_k^\dagger$ and c_k are, respectively, the magnon creation and annihilation operators, ω_k is the frequency of a magnon with wave number k, and the last term represents the interactions of magnons among themselves and with other elementary excitations in the crystal, such as phonons, electrons, plasmons, etc. The magnon interactions are responsible for the scattering processes that account for the magnon energy renormalization and relaxation, or damping, and consequently for its finite lifetime. In addition, they provide the means for the nonlinear dynamic interactions among magnons and other excitations, leading to very interesting phenomena [9,12]. For the renormalization of the magnon energies the important interaction is the one describing four-magnon scattering due to the exchange interaction, given by [3,9]

$$\mathrm{H_{exc}^{(4)}} = \frac{zJ}{4N} \sum_{\substack{k_1,k_2,\\ k_3,k_4}} \Delta(\vec{k})\,[\gamma(\vec{k}_1) + \gamma(\vec{k}_2) + \gamma(\vec{k}_3) + \gamma(\vec{k}_4) - 4\gamma(\vec{k}_4 - \vec{k}_1)]\; c_{k_1}^\dagger c_{k_2}^\dagger c_{k_3} c_{k_4}, \tag{2}$$

where z is the number of nearest neighbors of a spin, N is the number of spin in the crystal, J is the parameter of the exchange interaction, and $\gamma(\vec{k})$ is the structure factor defined by

$$\gamma_k = \frac{1}{z} \sum_{\vec{\delta}} e^{i\vec{k}\cdot\vec{\delta}}, \tag{3}$$

where $\vec{\delta}$ denotes the vector connecting a spin to its z nearest neighbors. Due to the $1/N$ factor in Eq. (2), the interaction energy is much smaller than the free-magnon energy. However, magnons are bosons, and in thermal equilibrium they have population given by the Bose-Einstein distribution:

$$\langle n_k \rangle = \frac{1}{e^{\hbar\omega_k/k_BT} - 1}, \tag{4}$$

where k_B is the Boltzmann constant and T the temperature. As the temperature increases and becomes a sizable fraction of the Curie temperature, the number of magnons increases and the magnon interaction becomes appreciable. Thus, one effect of the increase in temperature is a change in the magnon energy. The magnon energy renormalization can be calculated by writing the four-magnon Hamiltonian in Eq. (2) approximately in the quadratic form that contains the energy correction. Consider the Hamiltonian (2) for only two modes, the magnon of interest with wave vector $\vec{k}$ and another magnon $\vec{k}'$. Since $\vec{k}$ and $\vec{k}'$ can be any of the four wave vectors in Eq. (2), using the random-phase approximation, $c_{k'}^\dagger c_{k'} \to \langle c_{k'}^\dagger c_{k'} \rangle = \langle n_{k'} \rangle$, we can write the Hamiltonian (2) as

$$\mathrm{H_{exc}^{(4)}} = \sum_k \hbar\Delta\omega_k\, c_k^\dagger c_k, \tag{5}$$

where

$$\hbar\Delta\omega_k = -\frac{2zJ}{N} \sum_{k'} (1 + \gamma_{k-k'} - \gamma_k - \gamma_{k'})\,\langle n_{k'} \rangle \tag{6}$$

is the energy renormalization of the k magnon due to the four-magnon interaction. Notice that the random-phase approximation in a Hamiltonian for three-magnon interaction does not lead to a form like Eq. (5), so that it does not contribute to the energy renormalization [3,9]. For this reason, we did not consider in Eqs. (5) and (6) the three-magnon interaction arising from the dipolar energy. Equation (6) shows that as the temperature increases, the k magnon energy decreases because the number of thermal magnons k' increases. We shall make calculations assuming a spherical Brillouin zone and considering for the acoustic magnon branch the approximate dispersion relation

$$\omega_k = \omega_{\mathrm{ZB}} \left(1 - \cos\frac{\pi k}{2k_m}\right), \tag{7}$$

where ω_{ZB} is the zone boundary frequency and k_m is the radius of the spherical Brillouin zone. As shown in Refs. [9,45], expression (7) represents quite well the dispersion relation of the acoustic branch in YIG measured by inelastic neutron scattering with $\omega_{\mathrm{ZB}}/2\pi = 8$ THz. Since the sphere is an approximation to the actual Brillouin-zone boundary, k_m can be considered an adjustable parameter, so as to provide good fits of theory to experimental data. Replacing the sum over wave vectors by an integral in k space in Eq. (6), using $2zJ = \hbar\omega_{\mathrm{ZB}}/S$, and considering a spherical Brillouin zone with radius k_m, the change in energy of the k magnon becomes

$$\hbar\Delta\omega_k = \frac{\hbar\omega_{\mathrm{ZB}}\,(k_m a)^3}{2\pi^2 S} \int_0^1 q^2\,dq\,\frac{(1 + \gamma_{k-q} - \gamma_k - \gamma_q)}{e^x - 1}, \tag{8}$$

where $x = \hbar\omega_k/k_BT$ is the normalized energy and $q = k/k_m$ is the normalized wave number, which varies from 0 to 1. In order to obtain Eq. (8), the dependence of the integrand on the angle between the wave vectors was neglected and the integration on the polar and azimuthal angles was freely evaluated. For each temperature the integral in (8) was evaluated numerically by a discrete sum over a spherical Brillouin zone, considering the unrenormalized frequencies given by the dispersion relation in Eq. (7) and the corresponding geometric factor, and with the approximation $\gamma_{k-q} = \gamma_k\gamma_q$. The numbers used for YIG are $S = 5/2$, $\omega_{\mathrm{ZB}}/2\pi = 8.0$ THz, and $k_m a = 3.0$ (a is the lattice parameter), which are the values that give a good fit of theory to the magnetization data, as will be shown later.

In the first cycle of the evaluation of $\Delta\omega_k$, the frequencies and the Bose factors are calculated for each point k in the Brillouin zone without renormalization. In the following cycles the Bose factors are calculated with the magnon frequencies $\omega_k(T) = \omega_k(0) + \Delta\omega_k$, using $\Delta\omega_k$ from the previous cycle.

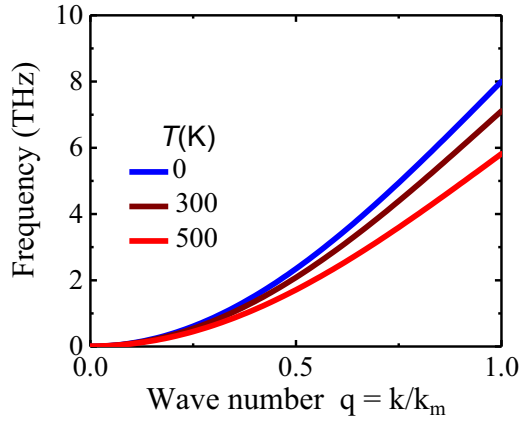

FIG. 1. Acoustic magnon dispersion relations in YIG at various temperatures, calculated with renormalization due to four-magnon exchange scattering.

The process is repeated until the change in frequency at all points is smaller than 0.1%. Figure 1 shows the calculated dispersions for three temperatures. Note that the curve for $T = 0$ K corresponds to the dispersion without magnon energy renormalization. From 0 to 300 K the zone-boundary magnon frequency reduces by about 12%, and from 300 to 500 K it reduces by an additional 18%. This variation is very similar to the one calculated for YIG with the full magnon dispersion and the exact Brillouin zone [58,59] that agrees with the neutron-scattering data [52]. As shown in Ref. [45], it is crucial to consider the renormalization of the magnon energies in the calculation of the temperature dependence of the magnetization to explain the experimental data.

III. TEMPERATURE DEPENDENCE OF SMALL WAVE-NUMBER MAGNON FREQUENCY AND COMPARISON WITH THEORY

Inelastic light-scattering techniques, Brillouin and Raman, provide powerful tools to measure the temperature dependence of the energy of zone-center magnons, phonons, and other elementary excitations in solids [61–64]. Here, we have used Brillouin light scattering (BLS) to measure the variation of the energy of small wave-number magnons in YIG. The experiments were performed with a bulk single-crystal YIG sample, cut into the shape of a rectangular prism with edges along ⟨100⟩ crystal axes, with dimensions $6.0 \times 3.0 \times 1.0$ mm^3 having the two large surfaces optically polished. The BLS measurements were done in the backscattering configuration, using a single-mode-stabilized Spectra Physics Excelsior diode pumped laser operating at 532 nm, with power 300 mW, attenuated by filters so that the power impinging on the sample was reduced to 15 mW. The laser beam was focused on one of the large sample surfaces by an $f/1.7$ camera lens that also collected the scattered radiation. The collimated scattered beam passed though a crossed analyzer and was focused into the entrance pinhole of a Sandercock TFP-1 tandem Fabry-Perot interferometer, operating in a (2×3)-pass configuration, with automatic control and data-acquisition board and software package.

To perform these measurements in a large temperature range it was necessary to build a temperature-control stage inside a vacuum chamber with a quartz optical window to allow transmission of the light from the laser beam and from the backscattering from the sample. Vacuum was necessary to prevent sample deterioration in measurements at high temperatures and condensation in cold ones. The sample was assembled tilted at an angle of 45 ° with respect to the incident laser beam and the temperature was measured through a thermocouple attached to the sample mount. The laser beam was focused onto the polished sample surface and the scattering light was collected to compose a spectrum at each temperature. Thermal equilibrium was reached after about 15 min for each temperature before starting scanning to acquire a spectrum. To ensure that the laser power had negligible effect on the sample temperature and did not generate a measurable change in frequency, we performed measurements to the laser-power dependence of the magnon frequency. The result was that in the laser power utilized in the experiments, the changes in frequency were negligible, being less than the error bars. All measurements were performed in the presence of an external magnetic field of 1.4 kOe applied along the larger sample edge and perpendicularly to the laser beam.

Figure 2(a) shows a typical spectrum measured with 5000 interferometer scans obtained with the sample temperature at 423 K and under an external magnetic field of 1.4 kOe. The full spectra in Fig. 2(b) show the frequency change of the Stokes and anti-Stokes peaks with sample temperature. Figures 2(c) and 2(d) show the data and Lorentzian function fits for Stokes and anti-Stokes peaks for some temperatures, demonstrating clearly the decrease in the magnon frequency with increasing temperature. For each temperature value one spectrum was acquired and fit with a Lorentzian function. The data points in Fig. (3) represent the frequencies extracted from the fittings of the peaks. Since the frequencies of the Stokes and anti-Stokes peaks are a little different due to the noise in the spectra, the data in Fig. 3 were determined by the averages of the Stokes and anti-Stokes frequencies and their differences are expressed by the error bars. In the backscattering configuration, the probed magnons have wave vector $\vec{k}$ perpendicular to the sample surface and to the applied magnetic field. The corresponding wave number is $k = 4\pi n/\lambda_L$, where n is the index of refraction and λ_L the laser wavelength. For the laser at 532 nm, with $n = 2.2$ for YIG, the magnon wave number is $k = 5.2 \times 10^5$ cm^{-1}, which corresponds to only 0.023 k_m. For this small wave number, in addition to exchange one has to consider the dipolar interaction. For spin waves propagating perpendicularly to the magnetic field, the free-magnon frequency is [1–9]

$$\omega_k = \gamma \left[(H_z + Dk^2)(H_z + Dk^2 + 4\pi M)\right]^{1/2}, \qquad (9)$$

where $\gamma = g\mu_B/\hbar$ is the gyromagnetic ratio, H_z is internal static magnetic field, related to the applied external field H_0 by $H_z = H_0 – N_z M$, where N_z is the demagnetizing factor, M is the magnetization, and $D = 2JSa^2/\gamma\hbar$ is the exchange parameter. In Eq. (9) we have neglected the magnetic crystalline anisotropy considered in Ref. [63] because its contribution to the magnon frequency in YIG is smaller than the error bars in Fig. 3.

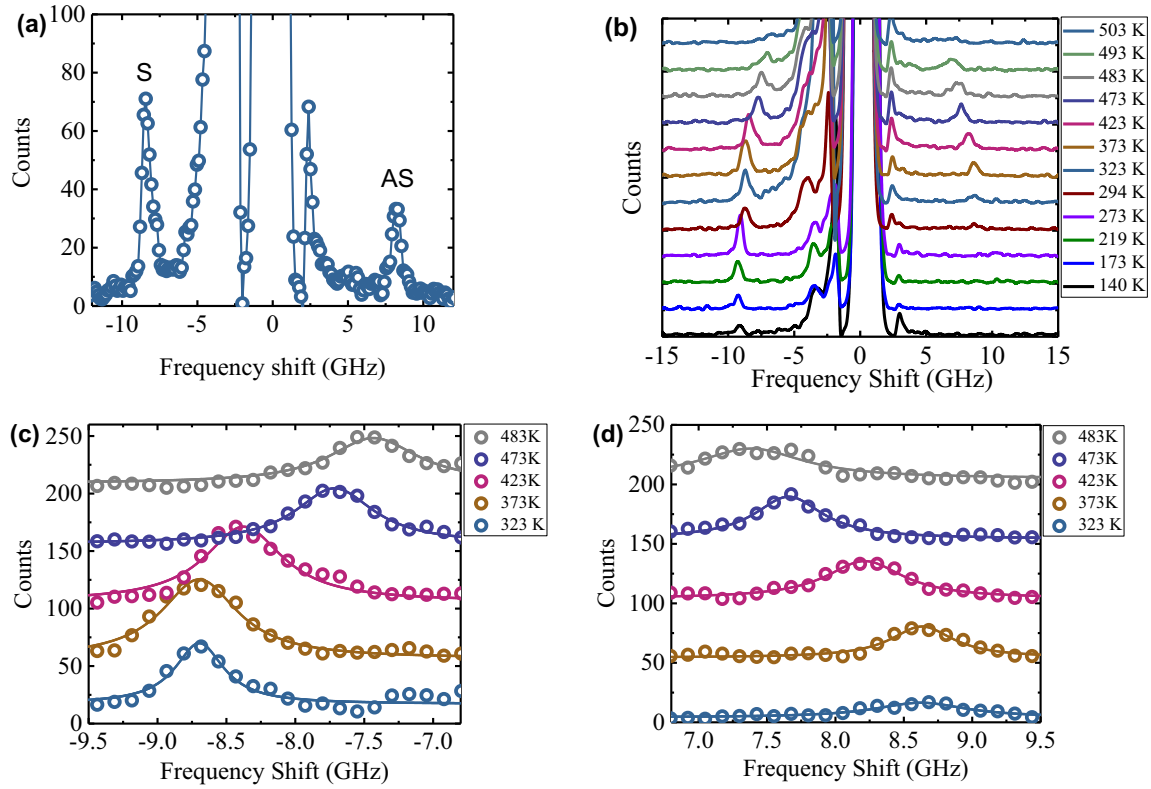

FIG. 2. (a) Full BLS spectrum measured with 5000 interferometer scans with the sample temperature at 423 K under an external magnetic field of 1.4 kOe. (b) Full BLS spectra for all measured temperatures. (c), (d) Zoom of some Stokes and anti-Stokes peaks with corresponding Lorentzian function fits.

Clearly, since the magnetization varies with temperature, the free-magnon frequency given by Eq. (9) also changes with temperature. The change in the magnon frequency measured by BLS in Ref. [65] was shown not to be completely accounted for by the temperature variation of the magnetization. This was interpreted as due to a nonequilibrium in the magnon system introduced by the probe laser. Here, we show that actually, the difference between the measured change in the magnon frequency with temperature and the one expected from the change in the magnetization is due to the magnon energy renormalization resulting from four-magnon scattering, as presented in Sec. II.

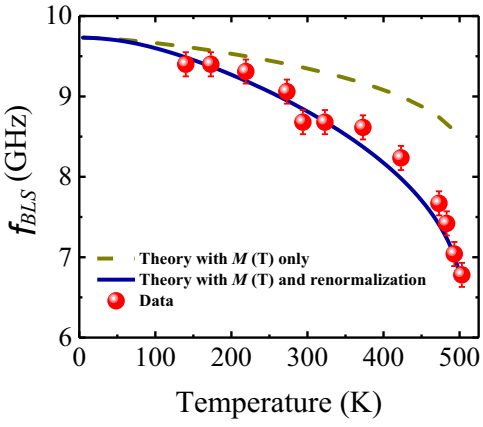

FIG. 3. Temperature variation of magnon frequency. Symbols represent data obtained with Brillouin light scattering. Dashed curve is a plot of Eq. (9) for $k = 5.2 \times 10^5$ cm^{-1}, $H_0 = 1.4$ kOe, and $M(T)$ measured experimentally in Refs. [66,67], and blue solid curve represents calculation taking into account magnon energy renormalization.

The dashed curve in Fig. 3 was obtained with Eq. (9) using for YIG the exchange parameter $D = 5.4 \times 10^{-9}$ Oe cm^2 and the temperature dependence of the magnetization measured experimentally and fit with a molecular-field model [66,67]. The magnetization data in the temperature range 0–500 K can also be explained quite well by spin-wave theory [9,45]. The value of the demagnetizing factor at the center of the large surface of the prism was obtained by the best fit of the full theory to data, as in the solid blue curve in Fig. 3, which gives $N_z = 0.1632$. Notice that this value is a little smaller than the one (0.1983) given by an analytic expression for the body center of a rectangular prism with aspect ratio $c/a = 2$ [68].

The solid curve in Fig. 3 represents the magnon frequency calculated with Eq. (9), added to the change in frequency due to renormalization evaluated numerically with Eq. (8) for the wave number of the magnon probed by BLS. Clearly, the magnon energy renormalization is crucial to explain the temperature dependence of the experimental data.

IV. CONCLUSION

In summary, we have presented an experimental study performed by Brillouin light-scattering technique to investigate

the temperature dependence of the acoustic magnon mode frequency in YIG over a wide temperature range. The change in the magnon frequency with temperature when just considering temperature dependence of the magnetization does not account for the full variation. In order to explain the experimental data it is necessary to use the theory of magnon energy renormalization. According to the theory, when the system temperature increases there is a distribution of magnon population through states, implying a correction in the magnon frequency due to magnon interactions. With this approach we obtain a quite good fit to the experimental data, confirming that the frequency change is not only governed by the temperature dependence of magnetization but also by magnon energy renormalization.

ACKNOWLEDGMENTS

The authors are grateful to V. J. da Silva and J. F. de Paula Filho for technical assistance. This work was supported by the Brazilian agencies Conselho Nacional de Desenvolvimento Científico e Tecnológico (CNPq), Coordenação de Aperfeiçoamento de Pessoal de Nível Superior (CAPES), Financiadora de Estudos e Projetos (FINEP), and Fundação de Amparo à Ciência e Tecnologia do Estado de Pernambuco (FACEPE).

[1] B. Lax and K. J. Button, *Microwave Ferrites and Ferrimagnetics* (McGraw-Hill, New York, 1962).
[2] M. Sparks, *Ferromagnetic Relaxation* (McGraw-Hill, New York, 1964).
[3] R. M. White, *Quantum Theory of Magnetism*, 3rd ed. (Springer-Verlag, Berlin, 2007).
[4] V. Cherepanov, I. Kolokolov, and V. L'vov, The saga of YIG: Spectra, thermodynamics, interaction and relaxation of magnons in a complex magnet, Phys. Rep. **229**, 81 (1993).
[5] A. G. Gurevich and G. A. Melkov, *Magnetization Oscillations and Waves* (CRC Press, Boca Raton, 1996).
[6] P. Kabos and V. S. Stalmachov, *Magnetostatic Waves and Their Applications* (Chapman and Hall, London, 1994).
[7] D. D. Stancil and A. Prabhakar, *Spin Waves- Theory and Applications* (Springer, New York, 2009).
[8] A. A. Serga, A. V. Chumak, and B. Hillebrands, YIG magnonics., J. Phys. D: Appl. Phys. **43**, 264002 (2010).
[9] S. M. Rezende, *Introducion to Magnonics*, Lecture Notes in Physics (Springer, Cham, 2020), Vol. 969, Chap. 6.
[10] S. M. Rezende and F. R. Morgenthaler, Magnetoelastic waves in time-varying magnetic fields, J. Appl. Phys. **40**, 524 (1969).
[11] P. Pirro, V. I. Vasyuchka, A. A. Serga, and B. Hillebrands, Advances in coherent magnonics, Nat. Rev. Mater. **6**, 1114 (2021).
[12] S. M. Rezende and F. M. de Aguiar, Spin-wave instabilities, auto-oscillations, and chaos in yttrium-iron-garnet, Proc. IEEE **78**, 893 (1990).
[13] B. A. Kalinikos, N. G. Kovshikov, and A. N. Slavin, Experimental observation of magnetostatic wave envelope solitons in yttrium iron garnet films, Phys. Rev. B **42**, 8658 (1990).
[14] M. Chen, M. A. Tsankov, J. N. Nash, and C. E. Patton, Backward-volume-wave microwave-envelope solitons in yttrium iron garnet films, Phys. Rev. B **49**, 12773 (1994).
[15] S. M. Rezende, F. M. de Aguiar, and O. F. de Alcantara Bonfim, Order and chaos in ferromagnetic spin wave instabilities, J. Magn. Magn. Mater. **54–57**, 1127 (1986).
[16] M. G. Cottam and A. N. Slavin, in *Linear and Nonlinear Spin Waves in Magnetic Films and Superlattices*, edited by M. G. Cottam (World Scientific, Singapore, 1994), Chap. 1.
[17] S. O. Demokritov, V. E. Demidov, O. Dzyapko, G. A. Melkov, A. A. Serga, B. Hillebrands, and A. N. Slavin, Bose–Einstein condensation of quasi-equilibrium magnons at room temperature under pumping, Nature (London) **443**, 430 (2006).
[18] V. E. Demidov, O. Dzyapko, S. O. Demokritov, G. A. Melkov, and A. N. Slavin, Observation of Spontaneous Coherence in Bose-Einstein Condensate of Magnons, Phys. Rev. Lett. **100**, 047205 (2008).
[19] S. M. Rezende, Theory of coherence in Bose-Einstein condensation phenomena in a microwave-driven interacting magnon gas, Phys. Rev. B **79**, 174411 (2009).
[20] B. Z. Rameshti, S. V. Kusminskiy, J. A. Haigh, K. Usami, D. Lachance-Quirion, Y. Nakamura, C.-M. Hu, H. X. Tang, G. E. W. Bauer, and Y. M. Blanter, Cavity magnonics, Phys. Rep. **979**, 1 (2022).
[21] R. W. Damon and H. Van de Vaart, Parametric amplification of magnetoelastic waves YIG at 8.7 Gc/sec, Appl. Phys. Lett. **6**, 152 (1965).
[22] Y. K. Fetisov, P. Kabos, and C. E. Patton, Active magnetostatic wave delay line, IEEE Trans. Magn. **34**, 259 (1998).
[23] I. C. Hunter and J. D. Rodhes, Electronically Tunable Microwave Bandpass Filters, IEEE Trans. Microwave Theory Tech. **30**, 1354 (1982).
[24] R. Suzuki, Recent development in magnetic-bubble memory, Proc. IEEE **74**, 1582 (1986).
[25] A. K. Zvezdin and V. A. Kotov, *Modern Magnetooptics and Magnetooptical Materials* (Taylor and Francis, New York, 1997).
[26] A. V. Chumak, A. A. Serga, and B. Hillebrands, Magnon transistor for all-magnon data processing, Nat. Commun. **5**, 4700 (2014).
[27] A. V. Chumak, V. I. Vasyuchka, A. A. Serga, and B. Hillebrands, Magnon spintronics, Nat. Phys. **11**, 453 (2015).
[28] C. Liu *et al.*, Long-distance propagation of short-wavelength spin waves, Nat. Commun. **9**, 738 (2018).
[29] Y. Kajiwara, K. Harii, S. Takahashi, J. Ohe, K. Uchida, M. Mizuguchi, H. Umezawa, K. Kawai, K. Ando, K. Takanashi, S. Maekawa, and E. Saitoh, Transmission of electrical signals by spin-wave interconversion in a magnetic insulator, Nature (London) **464**, 262 (2010).
[30] C. W. Sandweg, Y. Kajiwara, K. Ando, E. Saitoh, and B. Hillebrands, Enhancement of the spin pumping efficiency by spin wave mode selection, Appl. Phys. Lett. **97**, 252504 (2010).
[31] K. Ando, T. Na, and E. Saitoh, Nonlinear spin pumping induced by parametric excitation, Appl. Phys. Lett. **99**, 092510 (2011).
[32] L. H. Vilela-Leão, C. Salvador, A. Azevedo, and S. M. Rezende, Unidirectional anisotropy in the spin pumping voltage in

yttrium iron garnet/platinum bilayers, Appl. Phys. Lett. **99**, 102505 (2011).
[33] A. Hoffmann, Spin Hall effects in metals, IEEE Trans. Magn. **49**, 5172 (2013).
[34] J. Sinova, S. O. Valenzuela, J. Wunderlich, C. H. Back, and T. Jungwirth, Spin Hall effects, Rev. Mod. Phys. **87**, 1213 (2015).
[35] K. Uchida, J. Xiao, H. Adachi, J. Ohe, S. Takahashi, J. Ieda, T. Ota, Y. Kajiwara, H. Umezawa, H. Kawai, G. E. W. Bauer, S. Maekawa, and E. Saitoh, Spin Seebeck insulator, Nat. Mater. **9**, 894 (2010).
[36] K. Uchida, H. Adachi, T. Ota, H. Nakayama, S. Maekawa, and E. Saitoh, Observation of longitudinal spin-Seebeck effect in magnetic insulators, Appl. Phys. Lett. **97**, 172505 (2010).
[37] E. Padrón-Hernández, A. Azevedo, and S. M. Rezende, Amplification of Spin Waves by Thermal Spin-Transfer Torque, Phys. Rev. Lett. **107**, 197203 (2011).
[38] I. Zutic and H. Dery, Taming spin currents, Nat. Mater. **10**, 647 (2011).
[39] G. E. W. Bauer, E. Saitoh, and B. J. van Wees, Spin caloritronics, Nat. Mater. **11**, 391 (2012).
[40] L. Lu, Y. Sun, M. Jantz, and M. Wu, Control of Ferromagnetic Relaxation in Magnetic Thin Films through Thermally Induced Interfacial Spin Transfer, Phys. Rev. Lett. **108**, 257202 (2012).
[41] M. B. Jungfleisch, T. An, K. Ando, Y. Kajiwara, K. Uchida, B. I. Vasyuchka, A. V. Chumak, A. A. Serga, E. Saitoh, and B. Hillebrands, Heat-induced damping modification in yttrium iron garnet/platinum heterostructures, Appl. Phys. Lett. **102**, 062417 (2013).
[42] R. O. Cunha, E. Padrón-Hernández, A. Azevedo, and S. M. Rezende, Controlling the relaxation of propagating spin waves in yttrium iron garnet/Pt bilayers with thermal gradients, Phys. Rev. B **87**, 184401 (2013).
[43] M. Schreier, A. Kamra, M. Weiler, J. Xiao, G. E. W. Bauer, R. Gross, and S. T. B. Goennenwein, Magnon, phonon, and electron temperature profiles and the spin Seebeck effect in magnetic insulator/normal metal hybrid structures, Phys. Rev. B **88**, 094410 (2013).
[44] S. M. Rezende, R. L. Rodríguez-Suárez, R. O. Cunha, A. R. Rodrigues, F. L. A. Machado, G. A. Fonseca Guerra, J. C. Lopez Ortiz, and A. Azevedo, Magnon spin-current theory for the longitudinal spin-Seebeck effect, Phys. Rev. B **89**, 014416 (2014).
[45] S. M. Rezende, R. L. Rodríguez-Suárez, J. C. Lopez Ortiz, and A. Azevedo, Thermal properties of magnons and the spin Seebeck effect in yttrium iron garnet/normal metal hybrid structures, Phys. Rev. B **89**, 134406 (2014).
[46] J. Flipse, F. K. Dejene, D. Wagenaar, G. E. W. Bauer, J. Ben Youssef, and B. J. van Wees, Observation of the Spin Peltier Effect for Magnetic Insulators, Phys. Rev. Lett. **113**, 027601 (2014).
[47] S. Daimon, R. Iguchi, T. Hioki, E. Saitoh, and K. Uchida, Thermal imaging of spin Peltier effect, Nat. Commun. **7**, 13754 (2016).
[48] S. S. Costa and L. C. Sampaio, Recent progress in the spin Seebeck and spin Peltier effects in insulating magnets, J. Mag. Mag. Mat. **547**, 168773 (2022).
[49] H. Nakayama *et al.*, Spin Hall Magnetoresistance Induced by a Nonequilibrium Proximity Effect, Phys. Rev. Lett. **110**, 206601 (2013).
[50] M. Althammer, S. Meyer, H. Nakayama, M. Schreier, S. Altmannshofer, M. Weiler, H. Huebl, S. Geprägs, M. Opel, R. Gross *et al.*, Quantitative study of the spin Hall magnetoresistance in ferromagnetic insulator/normal metal hybrids, Phys. Rev. B **87**, 224401 (2013).
[51] S. Geller and M. A. Gilleo, Structure and ferrimagnetism of yttrium and rare-earth iron garnets, Acta Crystallogr. **10**, 239 (1957).
[52] J. S. Plant, Spinwave dispersion curves for yttrium iron garnet, J. Phys. C **10**, 4805 (1977).
[53] J. S. Plant, 'Pseudo-acoustic' magnon dispersion in yttrium iron garnet, J. Phys. C **16**, 7037 (1983).
[54] A. J. Princep, R. A. Ewings, S. Ward, S. Tóth, C. Dubs, D. Prabhakaran, and A. T. Boothroyd, The full magnon spectrum of yttrium iron garnet, npj Quantum Mater. **2**, 63 (2017).
[55] A. B. Brooks Harris, Spin-wave spectra of yttrium and gadolinium iron garnet, Phys. Rev. **132**, 2398 (1963).
[56] W. F. Brinkman and R. J. Elliott, Theory of spin-space groups, Proc. R. Soc. Lond. A **294**, 343 (1966).
[57] L.-S. Xie, G.-X. Jin, L. He, G. E. W. Bauer, J. Barker, and K. Xia, First-principles study of exchange interactions of yttrium iron garnet, Phys. Rev. B **95**, 014423 (2017).
[58] J. Barker and G. E. W. Bauer, Thermal Spin Dynamics of Yttrium Iron Garnet, Phys. Rev. Lett. **117**, 217201 (2016).
[59] J. Barker and G. E. W. Bauer, Semiquantum thermodynamics of complex ferrimagnets, Phys. Rev. B **100**, 140401(R) (2019).
[60] S. M. Rezende and J. C. Lopez Ortiz, Thermal properties of magnons in yttrium iron garnet at elevated magnetic fields, Phys. Rev. B **91**, 104416 (2015).
[61] D. R. Birt, K. An, A. Weathers, L. Shi, M. Tsoi, and X. Li, Brillouin light scattering spectra as local temperature sensors for thermal magnons and acoustic phonons, Appl. Phys. Lett. **102**, 082401 (2013).
[62] M. Agrawal, V. I. Vasyuchka, A. A. Serga, A. D. Karenowska, G. A. Melkov, and B. Hillebrands, Direct Measurement of Magnon Temperature: New Insight into Magnon-Phonon Coupling in Magnetic Insulators, Phys. Rev. Lett. **111**, 107204 (2013).
[63] L. Mihalceanu, V. I. Vasyuchka, D. A. Bozhko, T. Langner, A. Y. Nechiporuk, V. F. Romanyuk, B. Hillebrands, and A. A. Serga, Temperature-dependent relaxation of dipole-exchange magnons in yttrium iron garnet films, Phys. Rev. B **97**, 214405 (2018).
[64] K. S. Olsson, K. An, and X. Li, Magnon and phonon thermometry with inelastic light scattering, J. Phys. D: Appl. Phys. **51**, 133001 (2018).
[65] K. S. Olsson, K. An, X. Ma, S. Sullivan, V. Venu, M. Tsoi, J. Zhou, L. Shi, and X. Li, Temperature-dependent Brillouin light scattering spectra of magnons in yttrium iron garnet and permalloy, Phys. Rev. B **96**, 024448 (2017).
[66] E. E. Anderson, Molecular field model and the magnetization of YIG, Phys. Rev. **134**, A1581 (1964).
[67] P. Hansen, P. Röschmann, and W. Tolksdorf, Saturation magnetization of gallium-substituted yttrium iron garnet, J. Appl. Phys. **45**, 2728 (1974).
[68] A. Aharoni, Demagnetizing factors for rectangular ferromagnetic prisms, J. Appl. Phys. **83**, 3432 (1998).